Journal of Molecular Liquids 347 (2022) 118290

Contents lists available at ScienceDirect

Journal of Molecular Liquids

journal homepage: www.elsevier.com/locate/molliq

Molecular dynamic simulation and artificial intelligence of lead ions removal from aqueous solution using magnetic-ash-graphene oxide nanocomposite

Kunrong Zeng [a,*], Kadda Hachem [b], Mariya Kuznetsova [c], Supat Chupradit [d], Chia-Hung Su [e,*], Hoang Chinh Nguyen [f], A.S. El-Shafay [g,h,*]

[a] Department of Basic Science, Jiaozuo University, Jiaozuo, Henan 454003, China
[b] Laboratory of Biotoxicology, Pharmacognosy and Biological Valorization of Plants (LBPVBP), Faculty of Sciences, University of Saida – Dr Moulay Tahar, 20000 Saida, Algeria
[c] Department of Propaedeutics of Dental Diseases, Sechenov First Moscow State Medical University, Moscow, Russia
[d] Department of Occupational Therapy, Faculty of Associated Medical Sciences, Chiang Mai University, Chiang Mai 50200, Thailand
[e] Department of Chemical Engineering, Ming Chi University of Technology, New Taipei City, Taiwan
[f] Faculty of Applied Sciences, Ton Duc Thang University, Ho Chi Minh City 700000, Vietnam
[g] Department of Mechanical Engineering, College of Engineering, Prince Sattam bin Abdulaziz University, Alkharj, 16273, Saudi Arabia
[h] Mechanical Power Engineering Department, Faculty of Engineering, Mansoura University, Mansoura, 35516, Egypt

ARTICLE INFO

Article history:
Received 2 November 2021
Revised 30 November 2021
Accepted 6 December 2021
Available online 16 December 2021

Keywords:
Artificial intelligence
Molecular dynamics simulation
Adsorption
Lead ions
Magnetic nanocomposite

ABSTRACT

In this work, the heavy metal ions (lead, Pb) adsorption process were studied using an artificial intelligence simulation based model for prediction of the adsorption process by using magnetic ash/graphene oxide (GO) nanocomposite. Also, the adsorption mechanism of Pb ions on the adsorbent were investigated using molecular dynamics (MD) calculations in aqueous solution. Reactivity of structures, ionization energy (I), electron affinity (A), chemical hardness (η), chemical softness (σ), and energy gap (ΔE_{gap}) of all compounds were obtained from the HOMO–LUMO energy levels. The outcomes demonstrated that the adsorption of Pb ions on the adsorbent occurred through electrostatic interactions and van der waals bonding and the lead-water-GO configuration had the highest adsorption affinity according the ΔEgap calculations. The artificial neural network (ANN) with two hidden layers was used for developing the model with a mixture of linear and non-linear transfer functions. The equilibrium (Eq.) concentration of the Pb ion as an important factor in predicting the adsorption capacity of adsorbent was considered for the model output and initial Pb ion concentration as well as solution temperature were assumed as the model inputs. The training and validation procedure of ANN indicated great agreement between the experimental and predicted data according to the high coefficient of determination and low root mean square error (R^2 > 0.999, RMSE = 0.086). Based on the simulation results increasing the initial concentration of Pb ion significantly affect the Eq. concentration while the solution temperature had a lower effect on Eq. concentration. The results of this study provide valuable model for pollutants removal. MD calculations and artificial intelligence simulation methods could be an appropriate combined technique for predicting the adsorption behavior of nanocomposite in heavy metal ions removal from the aqueous solution with high accuracy.

1. Introduction

Till recent years, it was observed that domestic wastewaters contain a variety of dangerous contaminants such as heavy metals, pharmaceuticals, and dyes [1–3]. Heavy metals mainly appeared in the industrial wastewater from metal plating industries, pesticides, mining, nickel batteries, tanneries, organic chemicals, and lumber [4,5]. The accumulation of these pollutants in surface waters can be a result of imperfect treatment of wastewater and also slow

* Corresponding authors at: Department of Basic Science, Jiaozuo University, Jiaozuo, Henan 454003, China (K. Zeng) Department of Chemical Engineering, Ming Chi University of Technology, New Taipei City, Taiwan (C. H. Su) Department of Mechanical Engineering, College of Engineering, Prince Sattam bin Abdulaziz University, Alkharj, 16273, Saudi Arabia (A. S. El-Shafay).
E-mail addresses: ayaya2021123@163.com (K. Zeng), chsu@mail.mcut.edu.tw (C.-H. Su), a.abdou@psau.edu.sa (A.S. El-Shafay).

https://doi.org/10.1016/j.molliq.2021.118290
0167-7322/

natural deterioration which lead to harmful issues to human health and environment. Toxic metals such as cadmium (Cd(II)), copper (Cu(II)), lead (Pb(II)) and nickel (Ni(II)) ions can be accumulated in the human body and become toxic at high concentrations. It was proven that the certain amount of these ions cause kidney, brain and liver damage, chronic asthma and Wilson disease [5–7]. Several methods have been stated to remove heavy metals from wastewater including precipitation, electrochemical reduction, flotation, ion exchange, reverse osmosis, biological and membrane processes [8–15]. Many studies revealed the high capital costs and low efficiency performance of these methods in removal of small concentration of heavy metals. Among various chemical and physical technologies, adsorption process can be count as one of the most effective processes for wastewater treatment [5,16–18]. Adsorption technique has the highest impact on transport of heavy metals even at trace levels to its high efficiency, low cost, versatility, and simplicity. Different adsorbents have been applied in contaminant removal from wastewater [19]. It is seriously important to finding an available, low cost, and effective adsorbent. According to literature many inexpensive industrial or agricultural waste adsorbents such as wood, potato peels, sawdust, biochar have been used for heavy metal removal from aqueous solutions [20–22]. Normally, these materials are locally available and conversion of these resources to potential adsorbents would reduce the total costs of processes. Among these natural adsorbents fly ash from different resources have been tried successfully in removal of heavy metals and other organic contaminants from wastewater [23,24]. Recently, there is a growing attraction in production of nanocomposites with improved properties for different applications [25–33]. In order to increase the adsorption capacity of fly ash it can be composite with other adsorbents like graphene oxide (GO) as carbon-based nanomaterials [34–37]. Due to the effective oxygen groups in the GO structure, the surface of GO became hydrophilic which improve its ability in contaminant removal [38,39]. Also, the high surface area and electron density as well as easy combinability with different materials make GO as perfect candidate.

During last years, the application of magnetic materials in adsorption processes has gained much attention due to the recovery advantage which can separate them easily by a magnetic field at the end of the processes [40–43]. This can reduce the separation and recycling costs. For example Chen et. al [44] used multiwall carbon nanotube/iron oxide magnetic composites to remove Ni (II) and Sr(II) from aqueous media. As reported the adsorption capacity of the magnetic composites was significantly improved compared multiwall carbon nanotube and iron oxide. Moreover, the high adsorption capacity and surface area of iron oxide (Fe_3O_4) nanoparticles make it an effective active phase for ash/GO nanocomposite [45]. Studies on adsorption of heavy metal effluents have been conducted in many researches by experimental point of view but it is very important to provide a higher insight about the adsorption process and interaction between the pollutant and adsorbent. Developing a predictive model for design of novel materials with high adsorption capacity and optimization of adsorption process can be very helpful [42,46–49]. Moreover, development of predictive models can help design novel adsorbents with high adsorption capacity [50–52]. The machine learning (ML) method as one of the soft computing methods can be an excellent method for gaining valuable information about process simulation and optimization [53,54]. ML methods works according the big data of training a network and use of this trained network in simulation of process. Training of ML is according the experimental values. The artificial neural network (ANN) is a soft computing model which is successfully used for predicting the adsorption process and removal of heavy metal ions [8,54,55]. In a glance artificial intelligence (AI) received considerable attention for simulation and optimization of adsorption processes using complex materials including nanoporous materials. Development of AI model not only minimize the operational costs but also the obtained model can be applied for the process scale up and finding the effective factors that affect the adsorption efficiency. Furthermore, the optimum conditions can be obtained to maximize the adsorption capacity by manipulation of effective elements.

In adsorption of contaminants from aqueous solutions computational studies can provide valuable to understand the interaction at molecular level [56,57]. Simulation of molecular dynamics (MD) is an excellent tool for understanding how molecules interact, adsorb, and transport at the molecular scale [53,58,59]. MD simulations provide a powerful means of studying the atomic behavior of contaminants decomposing, which is not possible to study experimentally. MD computations can also provide insight into pollutant decomposition in atomic level.

In the current study, for the first time the equilibrium concentration (C_e) of the Pb ions in the presence of magnetic ash/graphene oxide nanocomposite were determined in the aqueous environment through modeling and simulation studies. Also, the molecular dynamic simulations were performed via *Material Studio* software to provide a good insight about the mechanism interactions between Pb ions and nanocomposite adsorbent at the molecular levels. Simulations offer significant data about HOMO, LUMO and gap energies as well as hardness, and reactivity of the interactions between Pb ions and nanocomposite adsorbent. Moreover, in order to provide a high-performance model for predicting the equilibrium concentration of ions, the machine learning model was used for the first time. The model is based on artificial neural network with two hidden layers and two inputs including the initial concentration of Pb ion and temperature of solution. While the equilibrium concentration of the metal ion in the solution was considered as the simulated output of the ANN model.

2. Materials and method

2.1. Adsorption procedure

The experiments of Pb ions removal from aquatic media were performed in batch mode. In each experiments the effect of different operating parameters including temperature and the initial concentration of Pb ion in the solution on the removal process were studied. In order to find the equilibrium state of the system, the contact time was changed and samples were taken and analyzed at different times of treatment process based on previous research [60]. It is worth noting that the flame atomic absorption spectroscopy (FAAS, Shimadzu AAS-6300 model) analyzer was used to measure the Pb concentration. Moreover, a number of adsorption isotherms were used for fitting the data of adsorption including Langmuir and Freundlich for the adsorption isotherms. In order to calculate the removal efficiency percent of Pb ions (R *(%)*):

$$R(\%) = \frac{C_i - C_e}{C_e} \times 100 \quad (1)$$

where the initial and equilibrium concentration of Pb ion presented as C_i and C_e. W is the amount of the magnetic nanocomposite in g and V is the volume of aquatic solution in L.

2.2. Dynamic molecular and quantum chemical calculations

The *Materials Studio* software was employed to analyze the molecular quantum calculations through DFTB$^+$ module. The *Hyperchem* software was used for initial geometry optimization of different structure including water, lead, and adsorbents (GO

and ash). Then, the DFTB$^+$ module was applied for the energy and geometry optimization as well as studying the HOMO and LUMO energy levels of components. After optimization of structures, the output file was used to be calculated by modules DFTB$^+$, Task; Geometry optimization, Quality: Fine, K-point set: Fine, Slater-Koster library: PBC & 3OB. In Population analysis the setting were as follow: Eigensolver: Divide and conquer and Total spin set as 1.

The obtained optimized configurations were used in Forcite modules and adsorption locator to predict the Pb adsorption on the GO and ash. In every calculation, a mixture of 12 molecules of heavy metals, five molecules of water and one molecule of adsorbent were simulated and the low energy configurations and energy distribution of the mixture were calculated. Fig. 1(a)-(d) shows the optimized structure of water, heavy metal ion (lead), GO, and ash obtained by *Materials Studio* software. The initial energy values of −2539.9, 995.9, and 91.6 kcal/mol are corresponded to the initial energy values of water, GO, and ash adsorbents, respectively. Although after geometry optimization, these values were changed to −2558.5, −6.5, and −1230.4 kcal/mol for water, GO, and ash adsorbents, respectively. As can be understand the total energies of these structures were reduced in the following order: GO > ash > water.

Descriptors of global reactivity describe the overall reactivity of a structure. Several quantum chemical descriptors can be used to predict the adsorption mechanism, including global hardness (η) and the inverse of hardness which is called softness (σ). As hardness of structure is defined as the resistance of a particle to changes in its electronic configuration, it can approximate the amount of charge transfer. The HOMO-LUMO gap is smaller in soft molecules, while it is much larger in hard molecules. Equations (2) and (3) can be used to calculate hardness and softness, respectively [53,57]:

$$\eta = \left(\frac{I - A}{2}\right) \tag{2}$$

$$\sigma = \frac{1}{\eta} \tag{3}$$

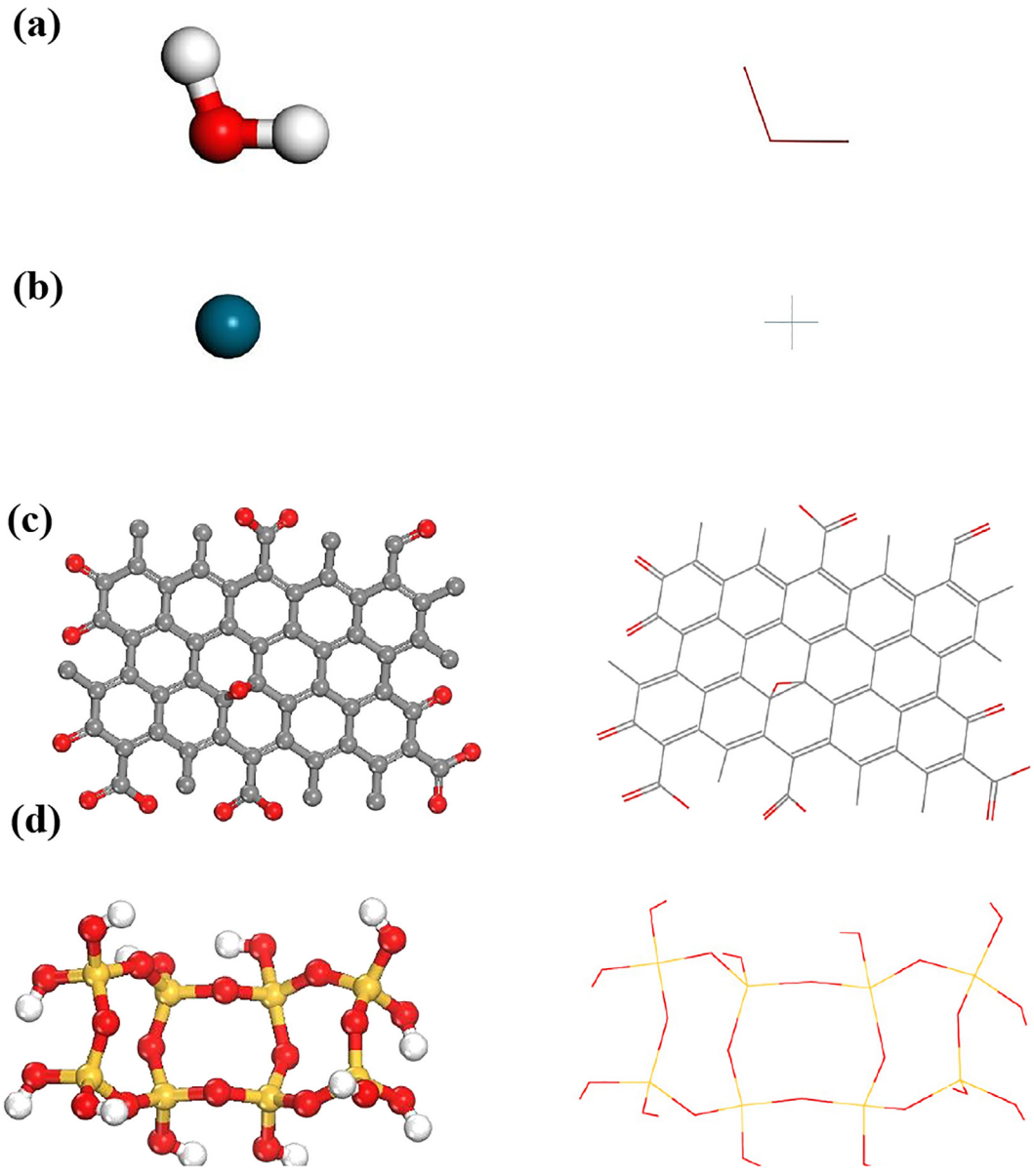

Fig. 1. The optimized structures of (a) water, (b) lead ion, (c) GO, and (d) ash.

According to these expressions, I and A are the electron affinity ($-E_{LUMO}$) and ionization potential ($-E_{HOMO}$), respectively.

2.3. Modeling and simulation of process

Simulation of data about the lead ion removal using magnetic nanocomposite was performed through a machine learning model using artificial neural network (ANN) method. Accordingly the prediction of the adsorption data was carried out developed by designing two hidden layers in which 2 non-linear (*TanH*), 1 linear, and 1 Gaussian functions are used in the hidden layers' nodes. The concentration at the equilibrium point (Eq.) was simulated in the model (the output parameter) which defines the equilibrium concentration (Ce) of the Pb ions. The *JMP* software was used for ANN calculations that can predict the output parameter and provide the relation of the input and output parameters. The simulation of the target value can be performed in *JMP* software by employing the multi-layer perceptron neural network. The structure of ANN model was optimized by trial and error via changing the type of network, activation functions, and node (as can be seen in Fig. 2). The model was established with two hidden layers which include linear and non-linear activation functions for predicting the Eq. concentration as output. The activation functions applied in the nodes were linear, TanH functions (Equation (4)), and Gaussian functions (Equation (5)):

$$\mathrm{TanH}\mathit{function} = \frac{e^{2x}-1}{e^{2x}+1} \tag{4}$$

$$\mathrm{Gaussian}\mathit{function} = \frac{n}{2}\left(\log(\mathrm{SSE}) + 1 + \log\left(\frac{2\pi}{n}\right)\right) \tag{5}$$

The Gaussian semi-log function based on the sum of squared errors (SSE) was used in the simulations. The number of used data was shown as n in the mentioned equation.

The ANN simulation of removal process was done in *JMP Pro 15* package. In this package one and two layers, fully connected, multilayer perceptron (MLP) network type can be properly fitted. The validation technique was performed using KFOLD and in all models K was 3. Table 1 listed the data points used in the simulations.

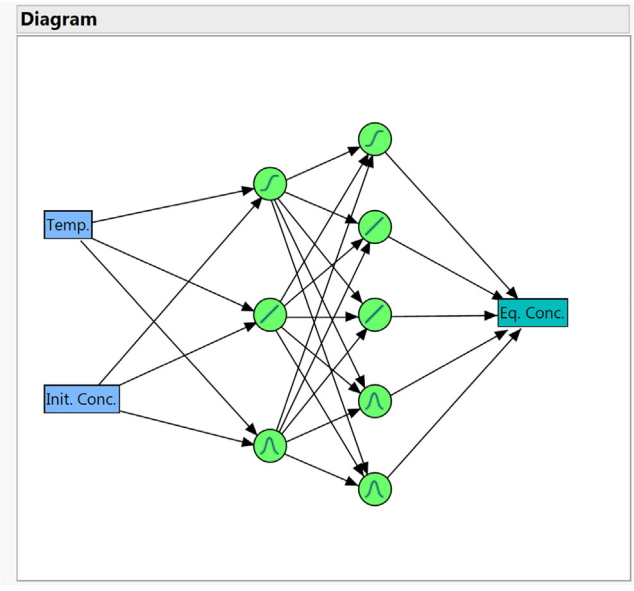

Fig. 2. The structure of ANN model used for prediction of lead ions adsorption.

3. Results and discussion

3.1. Adsorption capacity analysis

In the following of molecular dynamic simulations, the structures of water, heavy metal ion, and adsorbents were placed in a cell volume and optimized by DFTB$^+$ module. These simulation were performed to distinguish the appropriate location, energy values, and most stable adsorption of different configurations (heavy metal ion-water-adsorbent) [16]. The obtained results are shown in Fig. 3. The adsorption energy value of lead-water-GO configuration was about −52.6779 kcal/mol. In the lead-water-GO configuration, the lead ions in the cell interact with the GO structure through the oxygen atoms of GO. As it can be seen the distance between the lead ions and oxygen atoms of GO structure were around 3.16, 3.51, and 3.75 Å which confirmed that these interactions occurred through electrostatic.

Also, Fig. 4 shows the adsorption of lead ions on the ash surface in the presence of water molecules. According to the obtained results the adsorption energy value of lead-water-ash structure was about −27.0970 kcal/mol. Moreover, the adsorption of lead on this structure was occurred through hydrogen bonding and interaction of lead heavy metal ions with oxygen atoms of ash. The distance between these atoms of ash structure were around 3.95 and 3.99 Å which confirmed that the adsorption take place through the electrostatic interaction and van der waals bonding. It seems that the adsorption energy of lead-water-GO structure is more negative than lead-water-ash structure and this result indicated that graphene is stronger adsorbent compare to ash.

3.2. Frontier molecular orbital based analysis for different configurations

The frontier molecular orbital (FMO) theory is a very useful tool for description of highest occupied molecular orbitals (HOMO) and the lowest unoccupied molecular orbitals (LUMO) interactions and chemical reactivity of different structures. The HOMO often describe the electron donating ability of the component (nucleophilicity). On the other hand the LUMO often describe the electron accepting of the component (electrophilicity) [61]. The energy gap between LUMO and HOMO energy levels ($\Delta E_{GAP} = E_{LUMO}-E_{HOMO}$) provide valuable informations about the reactivity, stability of heavy metal ions-adsorbents configurations as well as evaluating the chemical reactivity of systems. The configurations with low E_{HOMO} and high E_{HOMO} values try to accept electrons from other donor configurations. ΔE_{GAP} represent the activity of structure and configurations with low ΔE_{GAP} have lower kinetic stability and higher chemical reactivity. Fig. 5 (a)-(c) shows the HOMO and LUMO energy levels and electron charge distributions of water molecule, ash and GO adsorbents. The HOMO energy level of water was calculated about −11.0612 eV and the LUMO energy level was obtained around −7.3881 eV. As shown in Fig. 5 (a), the HOMO energy levels of water were mainly positioned on the oxygen atom, whereas the LUMO energy levels were located largely on hydrogen atom. The HOMOs of ash and GO adsorbent are mostly centered on O atoms of ash and O of carbocyclic and hydroxyl groups of GO, respectively while the LUMOs are mainly localized on Si atoms of Ash and on rings of C element of GO fragments (Fig. 5 (b) and (c)). The calculated HOMO and LUMO values for the ash adsorbents were about −6.0483 eV and −0.4965 eV, respectively. Also, energy levels of −6.8433 and −9.9173 eV was obtained for LUMO and HOMO of GO adsorbent, respectively.

Also, the HOMO and LUMO distribution and values of configurations after adsorption of lead heavy metal ions on adsorbents were calculated based on the FMO theory in the presence of water mole-

Table 1
Lead ions adsorption data used in the simulations.

Number	Temp. (°C)	Initial conc. (mg/L)	Eq. Conc. (mg/L)	Predicted Eq. Conc. (mg/L)
1	30	5	0.0125	−0.1062
2	30	10	0.157	0.2629
3	30	20	0.654	0.5959
4	30	30	2.274	2.253
5	30	40	5.404	5.5902
6	30	50	8.665	8.6396
7	30	60	15.876	15.8849
8	30	70	24.136	24.1728
9	40	5	0.0643	0.0748
10	40	10	0.352	0.4411
11	40	20	0.934	0.9727
12	40	30	3.328	3.2420
13	40	40	7.214	7.2117
14	40	50	10.321	11.1083
15	40	60	17.591	16.2343
16	40	70	28.203	28.2268
17	50	5	0.123	0.21824
18	50	10	0.836	0.56639
19	50	20	1.112	1.2649
20	50	30	4.412	4.0530
21	50	40	8.543	8.5495
22	50	50	13.498	13.4618
23	50	60	19.349	19.3778
24	50	70	30.291	30.3163

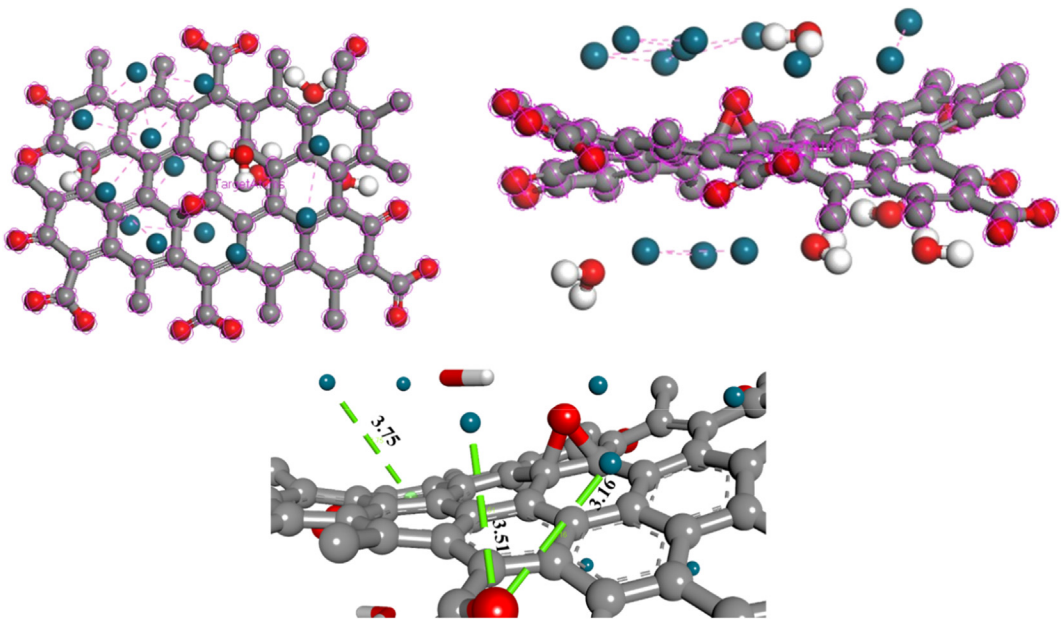

Fig. 3. Intermolecular and hydrogen interactions in the lead-water-GO configuration.

cules. The results of these calculations are presented in Fig. 6. From Fig. 6 (a) it can be inferred that the HOMO orbitals of lead-water-ash configuration were mostly positioned on lead ions and LUMO orbitals were localized on the O atoms of hydroxyl of ash structure. The HOMO and LUMO energy values of −7.9443 and −2.4741 eV were obtained for lead-water-ash configuration. The charge density of lead-water-GO configuration in Fig. 6 (b) demonstrated that the HOMOs were largely centered on a C ring of GO. Also, it can be seen that the LUMO orbitals of lead-water-GO configuration were largely localized on lead ions and O element of GO. The energy values of −8.7451 eV and −5.8086 eV in lead-water-GO were corresponded to the HOMOs and LUMOs, respectively.

The corresponding energy gaps between HOMO and LUMO (ΔE_{GAP}) for water, ash, and GO molecules were about 3.6731, 5.5518, and 3.074 eV, respectively. Also, ΔE_{GAP} for lead-water-ash and lead-water-GO configurations were obtained about 5.4702 and 2.9365 eV, respectively. Due to the lower HOMO–LUMO energy gap value of lead-water-GO configurations dye compared to lead-water-ash configurations, it can be concluded that the lead ions adsorption on the GO in composite structure is occurred easier due to high reactivity of GO molecule instead of ash.

3.3. Chemical hardness (η) and softness (σ) of compounds

When determining the reactivity of a structure, the chemical reactivity is of great importance. Molecules can be divided by their chemical reactivity into hardness (η) and softness (σ) molecules,

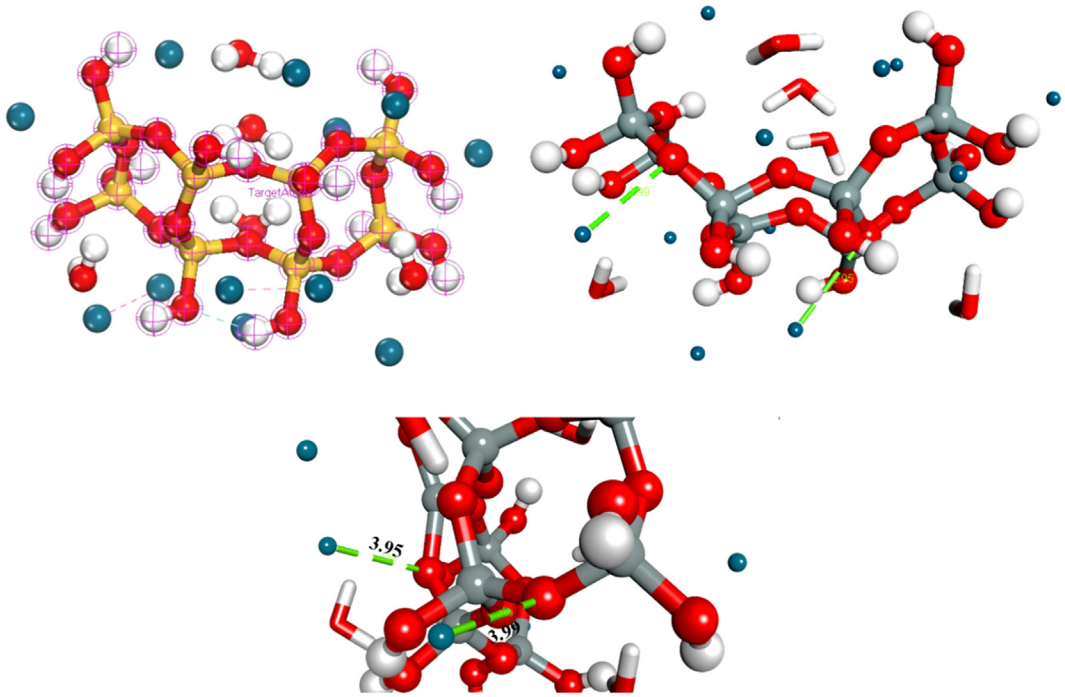

Fig. 4. Intermolecular and hydrogen interactions in the lead-water-ash configuration.

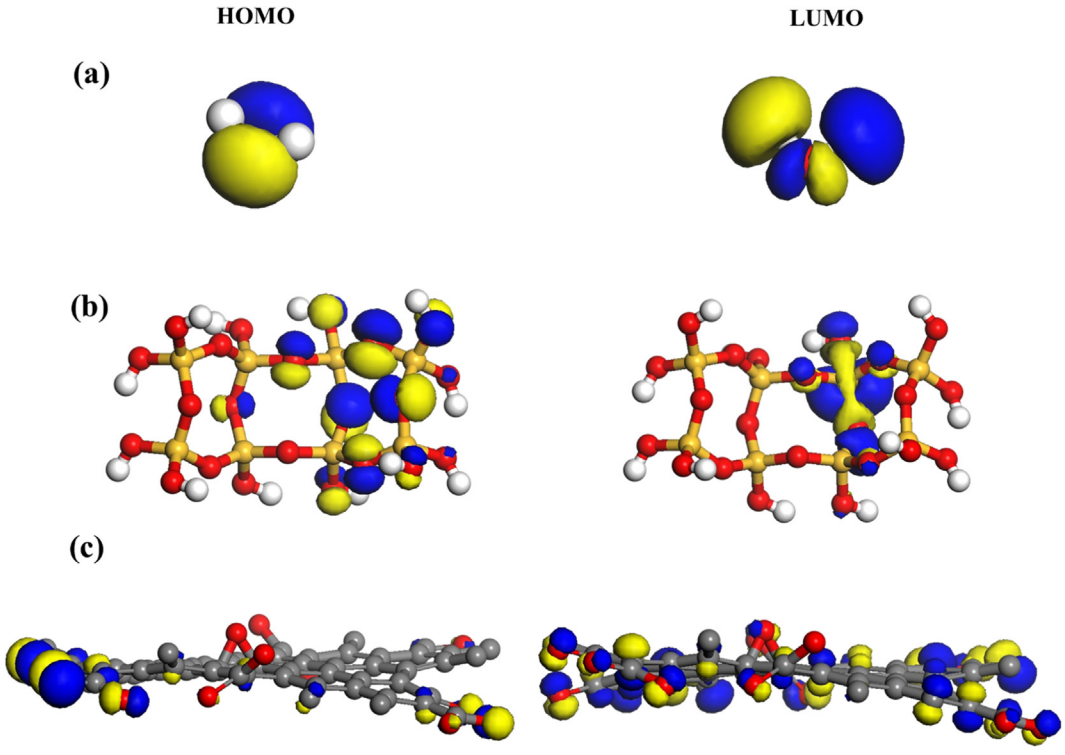

Fig. 5. The HOMO and LUMO for water (a), ash (b), and GO (c) structures.

and the hard molecules are less reactive than the soft ones. Physicochemical properties of chemical materials can be understood by considering their chemical hardness. Molecules with small/large energy gaps are called soft/hard molecules. As the E_{GAP} value increases, the chemical reactivity of structure decreases, and the stability increases [53].

The important chemical reactivity parameters were calculated via simulations for are titled configurations and the obtained results are listed in Table 2. According to Eqs. (3) and (4), hardness is inversely proportional to reactivity, i.e., a smaller value would mean more reactivity. The chemical hardness of water, ash, GO, lead-water-ash, and lead-water-GO configurations were about

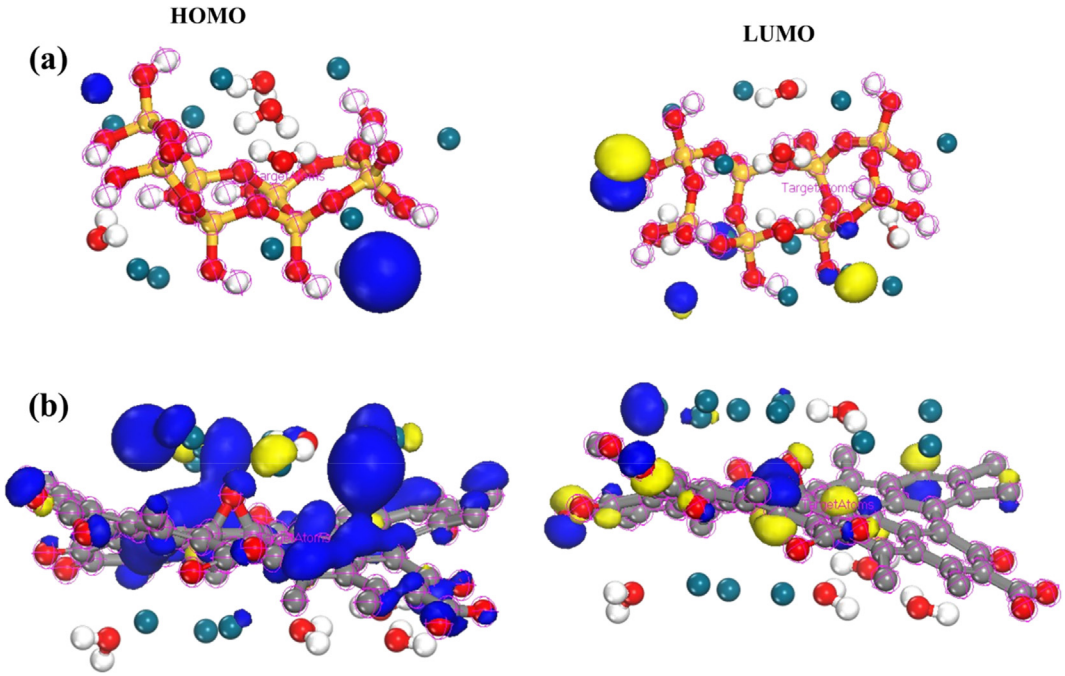

Fig. 6. The HOMO and LUMO for (a) lead-water-ash and (b) lead-water-GO configurations.

Table 2
Chemical reactivity factors obtained based on the simulation results.

Structure	HOMO	LUMO	ΔE_{gap}= $E_{LUMO} - E_{HOMO}$	I = $-E_{HOMO}$	A = $-E_{LUMO}$	$\eta = (\frac{I-A}{2})$	$\sigma = \frac{1}{\eta}$
water	−11.0612	−7.3881	3.6731	11.0612	7.3881	1.8365	0.5444
Ash	−6.0483	−0.4965	5.5518	6.0483	0.4965	2.7759	0.3602
GO	−9.9173	−6.8433	3.074	9.9173	6.8433	1.5370	0.6506
Lead-water-ash	−7.9443	−2.4741	5.4702	7.9443	2.4741	2.7351	0.3656
Lead-water-GO	−8.7451	−5.8086	2.9365	8.7451	5.8086	1.4682	0.6811

1.8365, 2.7759, 1.5370, 2.7351, and 1.4682 eV, respectively. Resulting from these values, the hardness of lead-water-GO was less than lead-water-ash configuration. Therefore it can be said, lead-water-GO configuration has less stability and is softer compare to lead-water-ash configuration. In conclusion, the chemical reactivity of GO was greater than that of ash in the presence of synthesis magnetic nanocomposite.

3.4. ANN simulation results

The obtained data from simulation of adsorption of lead ions by magnetic ash/ GO nanocomposite are presented in Tables 3 and 4 for the training and validation, respectively. These data obtained from artificial neural network model. Moreover the predicted values for Eq. concentration values versus the experimental data are presented and compared in Fig. 7 and the residual of fittings are shown in Fig. 8. As it can be confirm from the simulated data, there were great agreement between the predicted and the experimental results. The obtained results shown that the simulation using neural network model was adequate and acceptable, and the high determination coefficient (R^2 = 0.999) was obtained for training and validation of the network for the current study. Furthermore, according to the root mean square error (RMSE) and sum of squared errors (SSE) the model has been accurately trained and the model can simulate the process for lead ions removal from water by the synthesized magnetic ash/GO nanocomposite adsorbent.

Table 3
Analysis of training fitting.

Training, Eq. Conc.	
Measures	Value
RSquare	0.9999203
RMSE	0.086816
Mean Abs Dev	0.0583065
-LogLikelihood	−16.40042
SSE	0.1205922
Sum Freq	16

Table 4
Analysis of validation fitting.

Validation, Eq. Conc.	
Measures	Value
RSquare	0.9951564
RMSE	0.5766456
Mean Abs Dev	0.374441
-LogLikelihood	6.947289
SSE	2.6601612
Sum Freq	8

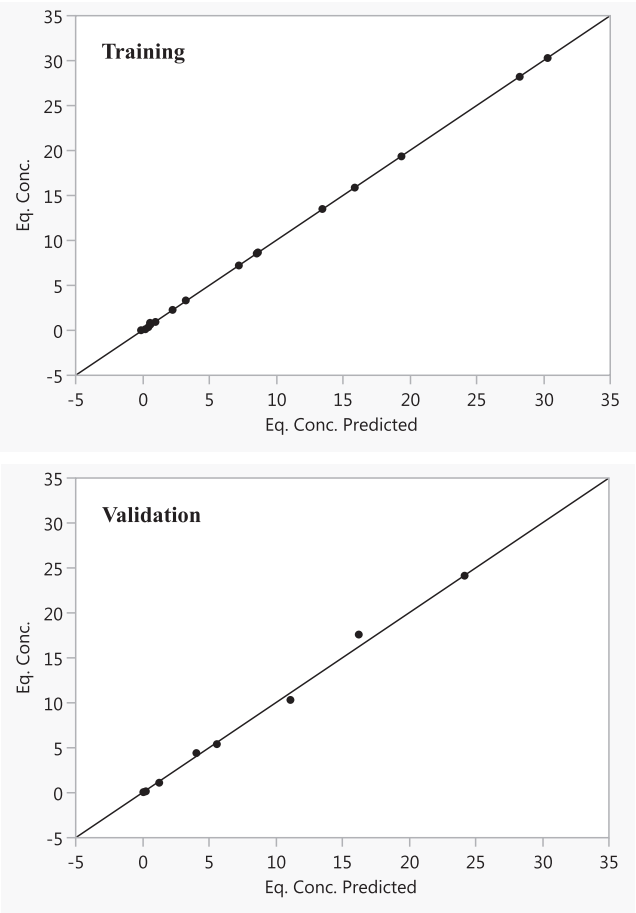

Fig. 7. Training and validation results obtained for the removal of Pb heavy metal ions.

The generated fitted and trained model was used in order to plot the predicted Eq. concentration versus initial concentration and temperature. The 3D and 2D representation of the simulated data are indicated in Fig. 9 and Fig. 10, respectively. As can be seen from Fig. 9 the initial concentration had a great effect on Eq. concentration and increasing the initial concentration led to an increment in Eq. concentration. In fact the initial content of ions can affect the driving force for mass transfer solute from the solution bulk to the magnetite adsorbent. Increasing the concentration of initial ions in the solution will increases the Eq. concentration meaningfully as predicted by the model. On the other hand, temperature had a lower effect on the Eq. concentration (Fig. 10). Increasing the temperature changed the Eq. concentration negligible. Moreover, for better understanding the surface plot and contour plot of the simulated data for predicting the Eq. concentration data versus initial concentration as well as temperature are presented in Fig. 11 and Fig. 12, respectively. Both of these plots confirmed the obtained results. The temperature increasing adversely affected the rate of the ion removal which is in agreement with the exothermic nature of the process. One of the reasons can be the changes and shrinkage of the produced nanocomposite adsorbent particles at higher temperature. This phenomenon reduce the number of the active sites and therefore lower amount of metal ions attached to the adsorbent surface. It is observed that there were a great agreement between the predicted and the observed removal data, which approve the strength and accuracy of the developed artificial neural network model in predicting the heavy metal ion removal process. According these results, it can be said that for improving the adsorption process, the initial concentration, and temperature should kept at their minimum amounts.

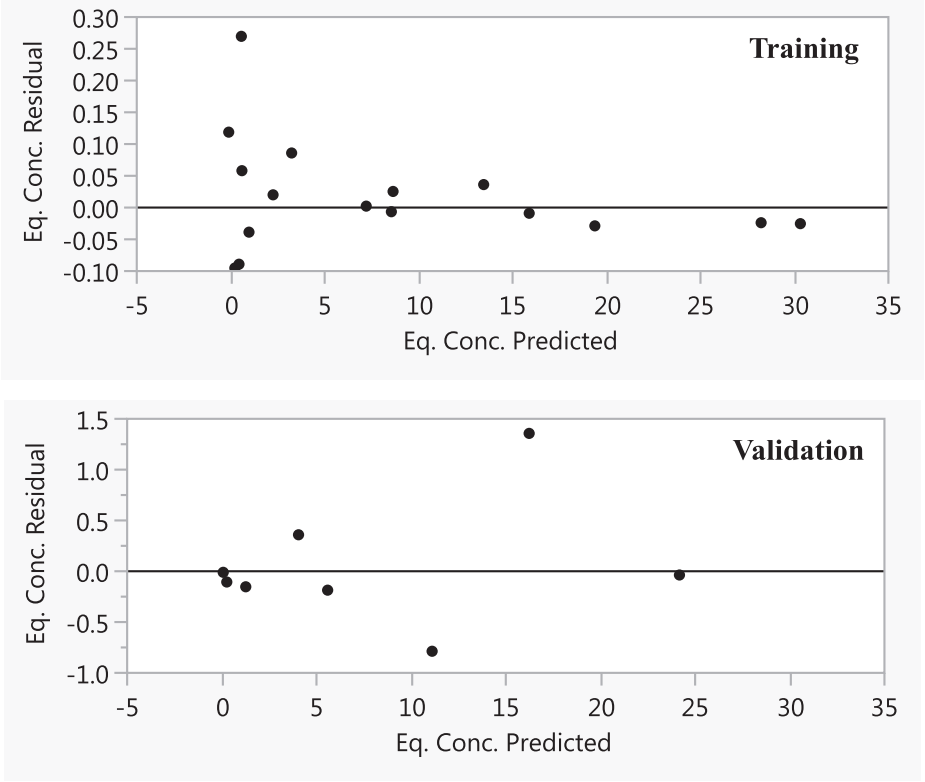

Fig. 8. Residual results obtained for the removal of Pb heavy metal ions.

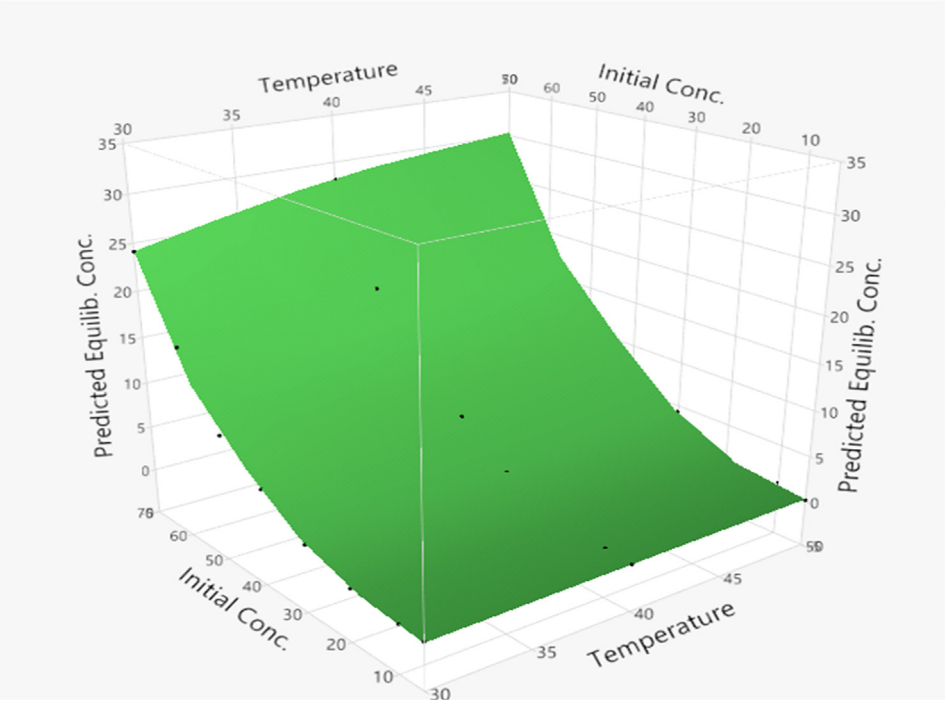

Fig. 9. 3D plot of predicted Eq. concentration versus initial concentration and temperature.

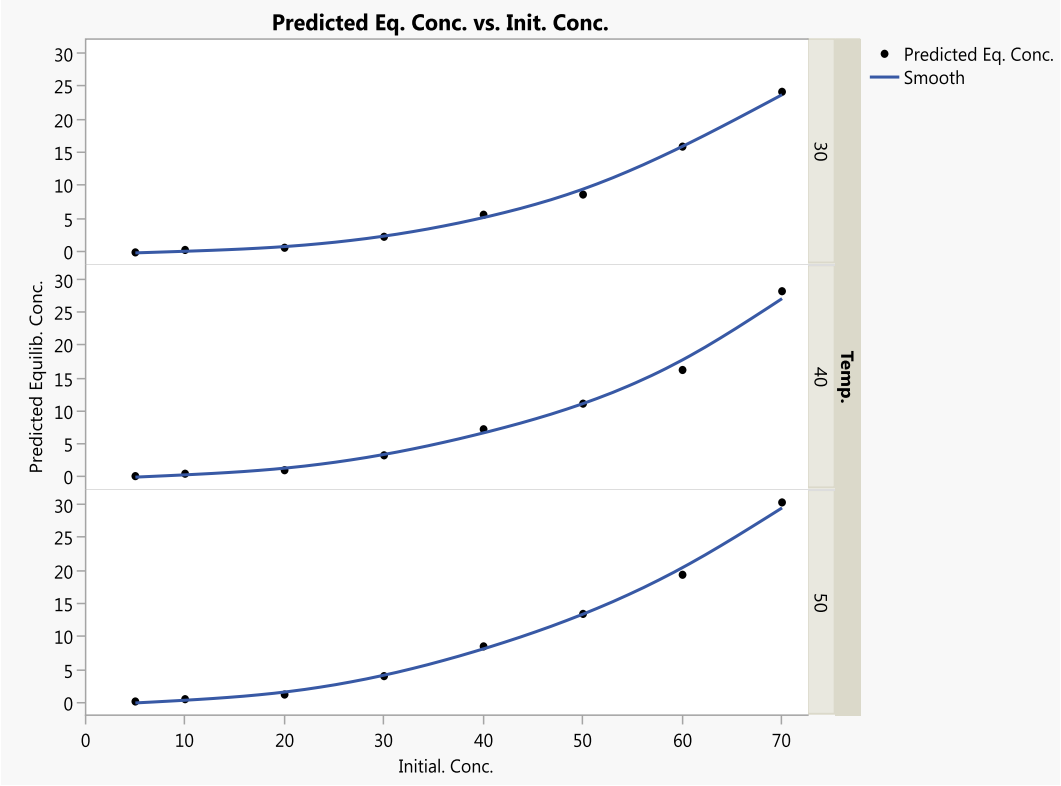

Fig. 10. 2D plot of predicted Eq. concentration versus initial concentration as well as temperature.

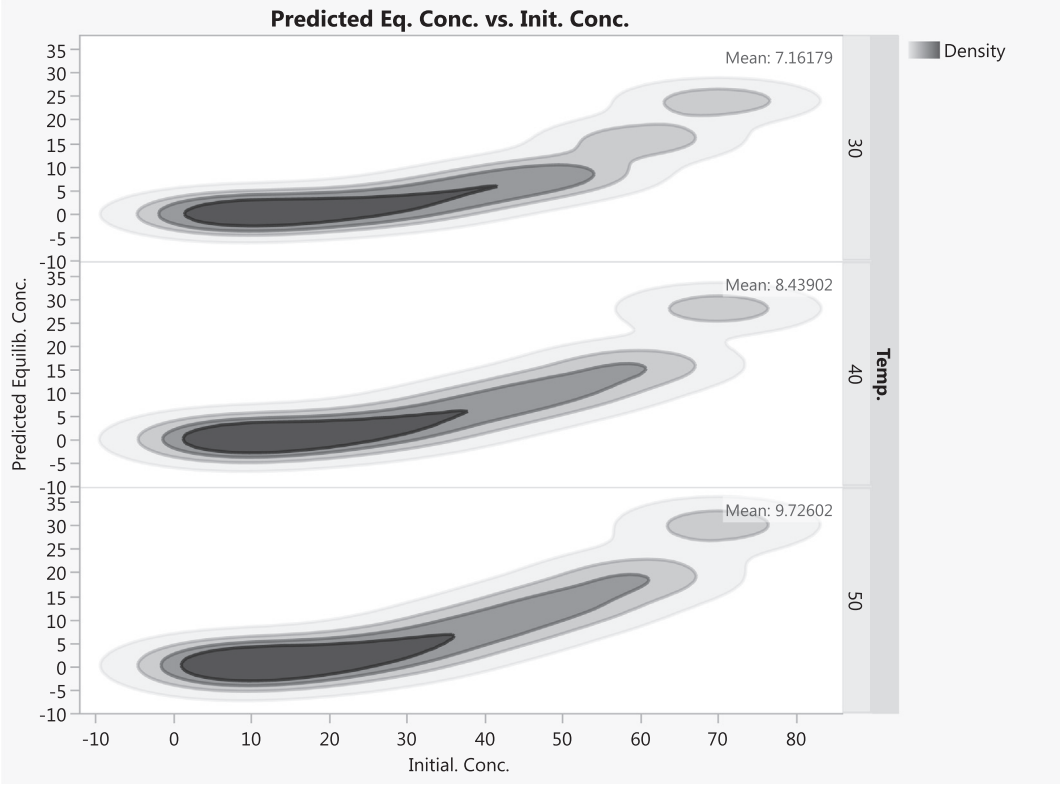

Fig. 11. Surface plot of predicted Eq. concentration versus initial concentration as well as temperature.

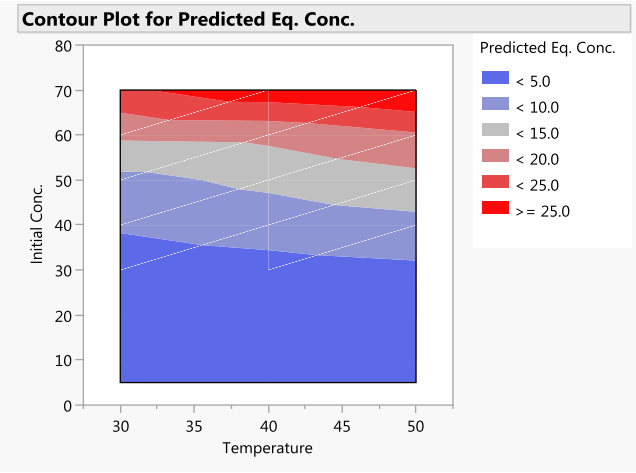

Fig. 12. Contour plot of predicted Eq. concentration using ANN.

4. Conclusions

In this study a machine learning based model was developed for simulation of adsorption process for removal of lead (Pb) ions from water solutions by using magnetic ash/GO nanocomposite. Molecular dynamic simulation were used to better understand the adsorption mechanism of lead heavy metal ions on the nanocomposites. The geometry of different structures were optimized by the DFTB$^+$ module and chemical reactivity, HOMO–LUMO energy levels, hardness, and softness were obtained using frontier molecular orbitals. The outcomes demonstrated that the adsorption of Pb ions on the adsorbent occurred through electrostatic interaction and van der waals bonding. Also, it can be concluded that the Pb ions adsorption on the GO in composite structure is occurred easier due to high reactivity of GO molecule instead of ash . Moreover, artificial intelligence was used to simulate the adsorption of Pb ions by nanocomposite and understanding the effect of different parameters on the adsorption process. The artificial neural network with two hidden layers were applied for developing the model with a mixture of linear and non-linear transfer functions. The initial concentration of Pb ion and the solution temperature were employed for training the neural network. The equilibrium concentration of Pb ion (C_e) sets as the output of model. The training and validation steps for simulation of Pb ions removal indicated a great accuracy and satisfactory with the high determination coefficient (R^2 > 0.999) for simulation of ion adsorption onto the surface of nanocomposite. The obtained model was assessed in prediction of equilibrium concentration, and revealed that increasing the initial concentration of heavy metal ions had a significant effect on the equilibrium concentration and Pb ion removal, while the initial temperature of solution does not change the equilibrium concentration significantly. This could be due to improvement in mass transfer driving force by increasing the ion initial concentration.

CRediT authorship contribution statement

Kunrong Zeng: Project administration, Writing – review & editing. **Kadda Hachem:** Investigation, Formal analysis, Validation. **Mariya Kuznetsova:** Writing – original draft, Conceptualization. **Supat Chupradit:** Validation, Investigation, Formal analysis. **Chia-Hung Su:** Methodology, Data curation. **Hoang Chinh Nguyen:** Validation. **A.S. El-Shafay:** Project administration, Writing – review & editing, Validation.

Declaration of Competing Interest

The authors declare that they have no known competing financial interests or personal relationships that could have appeared to influence the work reported in this paper.

Acknowledgement

Higher Vocational School Program for Key Teachers from Department of Education of Henan Province, China [2019GZGG042].

References

[1] Z. Heidari et al., Degradation of furosemide using photocatalytic ozonation in the presence of ZnO/ICLT nanocomposite particles: Experimental, modeling, optimization and mechanism evaluation, J. Mol. Liq. 319 (2020) 114193.
[2] R. Pelalak et al., High performance ozone based advanced oxidation processes catalyzed with novel argon plasma treated iron oxyhydroxide hydrate for phenazopyridine degradation, Sci. Rep. 11 (1) (2021) 1–18.
[3] S.S.M. Hassan et al., drug delivery systems between metal, liposome, and polymer-based nanomedicine: a review, European Chem. Bull. 9 (3) (2020) 91–102.
[4] K.S. Low, C.K. Lee, Cadmium uptake by the moss, *Calymperes delessertii Besch*, Bioresource Technol. 38 (1) (1991) 1–6.
[5] D. Lakherwal, Adsorption of heavy metals: a review, Int. J. Environ. Res. Development 4 (1) (2014) 41–48.
[6] J. Febrianto et al., Equilibrium and kinetic studies in adsorption of heavy metals using biosorbent: a summary of recent studies, J. Hazard. Mater. 162 (2–3) (2009) 616–645.
[7] G. Bereket, A.Z. Arog, M.Z. Özel, Removal of Pb(II), Cd(II), Cu(II), and Zn(II) from Aqueous Solutions by Adsorption on Bentonite, J. Colloid Interface Sci. 187 (2) (1997) 338–343.
[8] Z. Heidari et al., A new insight into catalytic ozonation of sulfasalazine antibiotic by plasma-treated limonite nanostructures: Experimental, modeling and mechanism, Chem. Eng. J. 428 (2022) 131230.
[9] R. Pelalak et al., Mathematical model for numerical simulation of organic compound recovery using membrane separation, Chem. Eng. Technol. 41 (2018) 345–352.
[10] H. Soltani et al., CFD simulation of transport phenomena in wastewater treatment via vacuum membrane distillation, J. Porous Media 19 (6) (2016) 515–526.
[11] A.K. Golder et al., Removal of hexavalent chromium by electrochemical reduction–precipitation: investigation of process performance and reaction stoichiometry, Sep. Purif. Technol. 76 (3) (2011) 345–350.
[12] H. Ozaki, K. Sharma, W. Saktaywin, Performance of an ultra-low-pressure reverse osmosis membrane (ULPROM) for separating heavy metal: effects of interference parameters, Desalination 144 (1–3) (2002) 287–294.
[13] H. Polat, D. Erdogan, Heavy metal removal from waste waters by ion flotation, J. Hazard. Mater. 148 (1–2) (2007) 267–273.
[14] G. Li et al., Defect-rich heterojunction photocatalyst originated from the removal of chloride ions and its degradation mechanism of norfloxacin, Chem. Eng. J. 421 (2021) 127852.
[15] G. Li et al., Near-infrared responsive upconversion glass-ceramic@ BiOBr heterojunction for enhanced photodegradation performances of norfloxacin, J. Hazard. Mater. 403 (2021) 123981.
[16] R. Pelalak et al., Molecular dynamics simulation of novel diamino-functionalized hollow mesosilica spheres for adsorption of dyes from synthetic wastewater, J. Mol. Liq. 322 (2021) 114812.
[17] A. Abbas et al., Heavy metal removal from aqueous solution by advanced carbon nanotubes: critical review of adsorption applications, Sep. Purif. Technol. 157 (2016) 141–161.
[18] A.E. Burakov et al., Adsorption of heavy metals on conventional and nanostructured materials for wastewater treatment purposes: A review, Ecotoxicol. Environ. Saf. 148 (2018) 702–712.
[19] R. Soltani et al., A water-stable functionalized NiCo-LDH/MOF nanocomposite: green synthesis, characterization, and its environmental application for heavy metals adsorption, Arabian J. Chem. 14 (4) (2021) 103052.
[20] T. Aman et al., Potato peels as solid waste for the removal of heavy metal copper (II) from waste water/industrial effluent, Colloids Surf., B 63 (1) (2008) 116–121.
[21] D.S. Malik, C.K. Jain, A.K. Yadav, Removal of heavy metals from emerging cellulosic low-cost adsorbents: a review, Appl. Water Sci. 7 (5) (2017) 2113–2136.
[22] Y. Zhou et al., Sorption of heavy metals on chitosan-modified biochars and its biological effects, Chem. Eng. J. 231 (2013) 512–518.
[23] I.J. Alinnor, Adsorption of heavy metal ions from aqueous solution by fly ash, Fuel 86 (5–6) (2007) 853–857.
[24] H. Cho, D. Oh, K. Kim, A study on removal characteristics of heavy metals from aqueous solution by fly ash, J. Hazard. Mater. 127 (1–3) (2005) 187–195.
[25] H. Ding et al., Enhancing strength-ductility synergy in an ex situ Zr-based metallic glass composite via nanocrystal formation within high-entropy alloy particles, Mater. Des. 210 (2021) 110108.
[26] M. Hu et al., Hierarchical dual-nanonet of polymer nanofibers and supramolecular nanofibrils for air filtration with high filtration efficiency, low air resistance and high moisture permeation, J. Mater. Chem. A (2021).
[27] Z. Zhang et al., Construction of pseudocapacitive Li2-xLaxZnTi3O8 anode for fast and super-stable lithium storage, Ceram. Int. 47 (1) (2021) 662–669.
[28] M. Wang et al., Reversible calcium alloying enables a practical room-temperature rechargeable calcium-ion battery with a high discharge voltage, Nat. Chem. 10 (6) (2018) 667–672.
[29] H. Guan et al., Chemical environment and magnetic moment effects on point defect formations in CoCrNi-based concentrated solid-solution alloys, Acta Mater. 187 (2020) 122–134.
[30] S.G. Al-Shawi et al., Synthesis of NiO nanoparticles and sulfur, and nitrogen co doped-graphene quantum dots/nio nanocomposites for antibacterial application, J. Nanostructures 11 (1) (2021) 181–188.
[31] J.P. Sonar et al., Synthesis and anti-proliferative screening of newthiazole compounds, European Chem. Bull. 9 (5) (2020) 132–137.
[32] M. Bashirzadeh, F.K. Behbahani, Green synthesis of quinoxaline derivatives at room temperature in ethylene glycol with H2SO4/SiO2 catalyst, Europ. Chem. Bull. 9 (1) (2020) 33–37.
[33] L. Mojtabavi, A. Razavi, The effects of addition of copper on the structure and antibacterial properties of biomedical glasses, Europ. Chem. Bull. 9 (1) (2020) 1–5.
[34] Q. Wang et al., Effect of fly ash on rheological properties of graphene oxide cement paste, Constr. Build. Mater. 138 (2017) 35–44.
[35] Y. Xie et al., Homogeneously dispersed graphene nanoplatelets as long-term corrosion inhibitors for aluminum matrix composites, ACS Appl. Mater. Interfaces 13 (27) (2021) 32161–32174.
[36] X. Zhang et al., A novel aluminum–graphite dual-ion battery, Adv. Energy Mater. 6 (11) (2016) 1502588.
[37] R. Pelalak, Z. Heidari, Lithographically cut multiwalled carbon nanotubes: opening caps, controlling length distribution, and functionalization, J. Dispersion Sci. Technol. 35 (6) (2014) 808–814.
[38] W. Peng et al., Adsorption of methylene blue on graphene oxide prepared from amorphous graphite: Effects of pH and foreign ions, J. Mol. Liq. 221 (2016) 82–87.
[39] G. Behbudi, Mini review of Graphene Oxide for medical detection and applications, Adv. Appl. NanoBio-Technologies 1 (3) (2020) 63–66.
[40] L. He et al., Novel coagulation waste-based Fe-containing carbonaceous catalyst as peroxymonosulfate activator for pollutants degradation: Role of ROS and electron transfer pathway, J. Hazard. Mater. 417 (2021) 126113.
[41] He, L., et al., Fe, N-doped carbonaceous catalyst activating periodate for micropollutant removal: Significant role of electron transfer. Applied Catalysis B: Environmental, 2021: p. 120880.
[42] C. Fu et al., Comprehensive investigations of mixed convection of Fe–ethylene-glycol nanofluid inside an enclosure with different obstacles using lattice Boltzmann method, Sci. Rep. 11 (1) (2021) 1–16.
[43] T.-C. Chen et al., Engineering of novel Fe-based bulk metallic glasses using a machine learning-based approach, Arabian J. Sci. Eng. 46 (12) (2021) 12417–12425.
[44] C. Chen et al., Adsorption behavior of multiwall carbon nanotube/iron oxide magnetic composites for Ni (II) and Sr (II), J. Hazard. Mater. 164 (2–3) (2009) 923–928.
[45] M. Salari, Optimisation using Taghuchi method and Heterogeneous Fenton-like Process with Fe3O4/MWCNTS Nano-Composites as the Catalyst for Removal an Antibiotic, Adv. Appl. NanoBio-Technol. 2 (3) (2021) 46–53.
[46] J. Qaderi, A brief review on the reaction mechanisms of CO2 hydrogenation into methanol, Int. J. Innovative Res. Scientific Studies 3 (2) (2020) 53–63.
[47] Y. Li et al., Point defect model for the corrosion of steels in supercritical water: Part I, film growth kinetics, Corros. Sci. 163 (2020) 108280.
[48] B. Bai et al., The attachment-detachment mechanism of ionic/nanoscale/microscale substances on quartz sand in water, Powder Technol. 394 (2021) 1158–1168.
[49] R. Pelalak et al., Efficient oxidation/mineralization of pharmaceutical pollutants using a novel Iron (III) oxyhydroxide nanostructure prepared via plasma technology: Experimental, modeling and DFT studies, J. Hazard. Mater. 411 (2021) 125074.
[50] S. Chupradit et al., Use of Organic and Copper-Based Nanoparticles on the Turbulator Installment in a Shell Tube Heat Exchanger: A CFD-Based Simulation Approach by Using Nanofluids, J. Nanomaterials 2021 (2021).
[51] Z. Tao et al., Finite difference modelings of groundwater flow for constructing artificial recharge structures, Iranian J. Sci. Technol. Trans. Civil Eng. (2021) 1–12.
[52] P. Zhu, H. Saadati, M. Khayatnezhad, Application of probability decision system and particle swarm optimization for improving soil moisture content, Water Supply (2021).
[53] Z. Heidari et al., Molecular modeling investigation on mechanism of cationic dyes removal from aqueous solutions by mesoporous materials, J. Mol. Liq. 329 (2021) 115485.
[54] R. Pelalak et al., Degradation of sulfonamide antibiotics using ozone-based advanced oxidation process: Experimental, modeling, transformation mechanism and DFT study, Sci. Total Environ. 734 (2020) 139446.

[55] N.G. Turan, B. Mesci, O. Ozgonenel, The use of artificial neural networks (ANN) for modeling of adsorption of Cu (II) from industrial leachate by pumice, Chem. Eng. J. 171 (3) (2011) 1091–1097.
[56] D.V. Chachkov, O.V. Mikhailov, Novel Modifications of Elemental Nitrogen ond Their Molecular Structures–A Quantum-Chemical Calculation, Europ. Chem. Bull. 9 (3) (2020) 78–81.
[57] R. Pelalak et al., Synthesis, molecular dynamics simulation and adsorption study of different pollutants on functionalized mesosilica, Sci. Rep. 11 (1) (2021) 1967.
[58] R. Sun et al., Defect engineering for high-selection-performance of NO reduction to NH3 over CeO2 (111) surface: a DFT study, Chin. Chem. Lett. (2021).
[59] Y. Cao et al., Molecular dynamic simulations and quantum chemical calculations of adsorption process using amino-functionalized silica, J. Mol. Liq. 330 (2021) 115544.
[60] R. Pelalak et al., Oak wood ash/GO/Fe3O4 adsorption efficiencies for cadmium and lead removal from aqueous solution: Kinetics, equilibrium and thermodynamic evaluation, Arabian J. Chem. 14 (3) (2021) 102991.
[61] Y. Kara, S. Sagdinc, A. Eşme, Theoretical study on the relationship between the molecular structure and corrosion inhibition efficiency of long alkyl side chain acetamide and isoxazolidine derivatives, Prot. Met. Phys. Chem 48 (2012) 710–721.